Micelle-to-Vesicle Transition of an Iron-Chelating Microbial Surfactant, Marinobactin E

Tate Owen,[†] Roger Pynn,[‡] Jennifer S. Martinez,[‡] and Alison Butler*,[†]

Department of Chemistry & Biochemistry, University of California, Santa Barbara, California 93106-9510, and Los Alamos National Laboratory, Los Alamos, New Mexico 87545

Received July 18, 2005. In Final Form: September 26, 2005

Small-angle neutron scattering (SANS) and dynamic light scattering (DLS) techniques have been applied to study the self-assembly processes of a microbially produced siderophore, marinobactin E (M_E). M_E is one of a series of marinobactins A−E that facilitate Fe(III) acquisition by the source bacterium through coordination of Fe(III) by the marinobactin headgroup. M_E is a six-amino-acid peptide amphiphile appended by palmitic acid (C_{16}), and differs only in the nature of the fatty acid moiety from the other marinobactins. Apo-M_E (uncoordinated M_E) assembles to form micelles with an average diameter of 4.0 nm. Upon coordination of one equivalent of Fe(III), the mean micellar diameter of Fe(III)−M_E shrinks to ∼2.8 nm. However, in the presence of excess Fe(III), Fe(III)−M_E undergoes a micelle-to-vesicle transition (MVT). At a small excess of Fe(III) over Fe(III)−M_E (i.e., <1.2 Fe(III)/M_E), a fraction of the Fe(III)−M_E micelles rearrange into ∼200 nm diameter unilamellar vesicles. At even greater Fe(III)/M_E ratios (e.g., 2−3) multilamellar aggregates begin to emerge, consistent with either multilamellar vesicles or lamellar stacks. The MVT exhibited by M_E may represent a unique mechanism by which marine bacteria may detect and sequester iron required for growth.

Introduction

Metal-chelating surfactants are attracting much attention, particularly in self-assembly processes.[1−5] Synthetic amphiphiles ranging from monodentate[1,5] to multidentate[2−4] metal-coordinating headgroups, as well as those containing single[1−3] or dual fatty acid tails,[4,5] form a diverse array of aggregate morphologies including micelles and vesicles[1−3] as well as stacked lamellae and multilamellar vesicles.[4,5] Changes in the ionic charge or molecular geometry of a surfactant upon coordination of a metal ion can induce dramatic phase changes. For example, single-tailed amphiphiles, which generally form micelles in solution, can be induced to form vesicles upon coordination of metal ion(s). Coordination of Cu(II), Co(II), or Ni(II) to micelles of hexadecyliminodiacetate ($C_{16}N(CH_2COO^-)_2$) induce vesicle formation in dilute aqueous solution.[2] Coordination of Ag(I) to octadecylamine ($C_{18}H_{37}NH_2$) induces a micelle-to-vesicle transition (MVT) resulting from a 2:1 ligand/Ag(I) stoichiometry.[1] Charged surfactant vesicles form upon addition of zinc dihydroperfluorooctanoate ($Zn(C_6F_{13}CH_2COO)_2$) to tetradecyldimethylamine oxide (C_{14}DMAO).[6] Complexation of Cu(II) triggers the conversion of the dual-tailed surfactant dihexadecyl-[5-(1-imidazolyl)-3-oxapentyl]-methylammonium ion, which forms planar bilayers in aqueous solution, to closed bilayer vesicles.[5] Furthermore, the recently reported MVT induced upon Fe(III) coordination to monopodal or tripodal catecholate surfactants (C_{14}−C_{16}; critical micelle concentrations (CMCs) < 10^{-5}) even offers a potential new approach to iron chelation therapy.[3] Thus, further elucidating the factors that govern MVTs is of enormous interest in not only nanotechnology, materials chemistry, and colloidal chemistry, but also in biochemistry and the pharmaceutical fields, among other areas.

While all of the above examples are synthetic amphiphiles, some bacteria produce metal-binding amphiphiles that display similar MVTs. The marinobactins A−E are a suite of siderophores produced by the marine bacterium, *Marinobacter* sp. DS40M6 to facilitate the acquisition of iron.[7,8] Siderophores are low molecular weight iron(III)-chelating compounds secreted by bacteria that can solublize colloidal iron oxide and have a very high stability constant for Fe(III).[9,10] The marinobactins each comprise the same six-amino-acid peptidic headgroup that coordinates Fe(III) but differ in the nature of the fatty acid appendage (C_{12}−C_{16}) (Figure 1).

The CMCs of marinobactins D and E (M_D and M_E), which are produced in the greatest amount and have the longest fatty acids, range between ∼50 and 75 μM, depending on a variety of factors, including pH and ionic strength as well as whether Fe(III) is coordinated.[7] In the presence of Fe(III), solutions of M_D form vesicles that are 100−200 nm in diameter, as observed by cryo-transmission electron microscopy (cryo-TEM) (Figure 2) and dynamic light scattering (DLS).[7] In the absence of iron(III), however, cryo-TEM and DLS reveal no evidence of vesicle formation for apo-M_D and apo-M_E (uncoordinated M_D and M_E). Thus,

* To whom correspondence should be addressed. E-mail: Butler@chem.ucsb.edu.

† University of California.

‡ Los Alamos National Laboratory.

(1) Luo, X.; Miao, W.; Wu, S.; Liang, Y. *Langmuir* **2002**, *18*, 9611−9612.

(2) Luo, X.; Wu, S.; Liang, Y. *Chem. Commun.* **2002**, *5*, 492−493.

(3) Apostol, M.; Baret, P.; Serratrice, G.; Desbrières, J.; Putaux, J.-L.; Stébé, M.-J.; Expert, D.; Pierre, J.-L. *Angew. Chem.* **2005**, *117*, 2636−2638.

(4) Sommerdijk, N. A. J. M.; Booy, K. J.; Pistorius, A. M. A.; Feiters, M. C.; Nolte, R. J. M.; Zwanenburg, B. *Langmuir* **1999**, *15*, 7008−7013.

(5) van Esch, J. H.; Stols, A. L. H.; Nolte, R. J. M. *J. Chem. Soc., Chem. Commun.* **1990**, 1658−1660.

(6) Hao, J.; Wang, J.; Liu, W.; Abdel-Rahem, R.; Hoffmann, H. *J. Phys. Chem. B* **2004**, *108*, 1168−1172.

(7) Martinez, J. S.; Zhang, G. P.; Holt, P. D.; Jung, H.-T.; Carrano, C. J.; Haygood, M. G.; Butler, A. *Science* **2000**, *287*, 1245−1247.

(8) Martinez, J. S.; Carter-Franklin, J. N.; Mann, E. L.; Martin, J. D.; Haygood, M. G.; Butler, A. *Proc. Natl. Acad. Sci. U.S.A.* **2003**, *100*, 3754−3759.

(9) Butler, A. *Science* **1998**, *281*, 207−210.

(10) Lewis, B. L.; Holt, P. D.; Taylor, S. W.; Wilhelm, S. W.; Trick, C. G.; Butler, A.; Luther, G. W., III *Mar. Chem.* **1995**, *50*, 179−188.

10.1021/la0519352 CCC: $30.25
Published on Web 11/12/2005

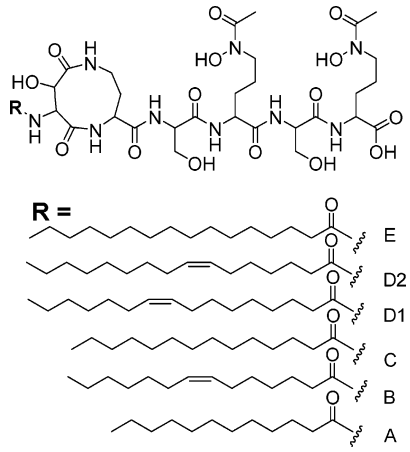

Figure 1. Structure of marinobactins A−E. Fe(III) coordination occurs via each bidentate hydroxamate group and the bidentate hydroxyamide moiety.

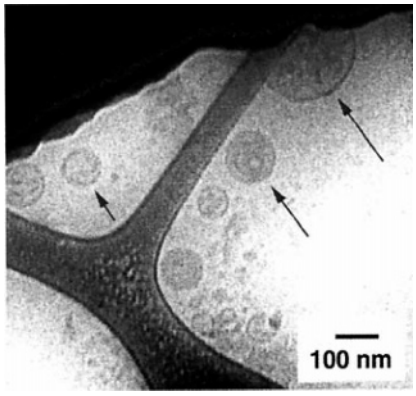

Figure 2. Cryoelectron micrograph of Fe(III)−M_D siderophore vesicles in aqueous solution. Representative vesicles are indicated by arrows. Reproduced from ref 7.

the iron(III)-induced MVT is an intriguing feature of these siderophores that may be advantageous in the microbial iron acquisition process.

Herein we report results of small-angle neutron scattering (SANS) and DLS to characterize the MVT of M_E in the presence of Fe(III). We find that, in aqueous solution, apo-M_E assembles to form micelles that decrease in size when one equivalent of Fe(III) coordinates to M_E. If the Fe(III) concentration exceeds the M_E concentration, the micelle population decreases, and evidence of vesicle formation is observed by both SANS and DLS. It is hypothesized that, when the iron concentration exceeds the M_E concentration, excess iron can bridge the anionic headgroups of several M_E molecules, drawing them closer together in an arrangement that favors vesicle formation.

Materials and Methods

Definitions. Fe(III)−M_E refers to marinobactin E coordinated to Fe(III). Apo-M_E indicates marinobactin E that is not coordinated to Fe(III).

Materials. Deuterium oxide, deuterium chloride, and sodium deuterioxide were purchased from Cambridge Isotope Laboratories, Inc. Triply deionized water (Barnstead NANOpure II) was used in all experiments. All other chemicals and organic solvents were purchased from EM Science. M_E was obtained from an aqueous bacterial culture (*Marinobacter* species strain DS40M6) and purified as previously described.[7,11]

Sample Preparation. D_2O was used as a solvent in place of H_2O to maximize the neutron scattering contrast between M_E and the solvent and to obtain an optimum signal for SANS measurements. All samples analyzed by DLS and SANS consisted of 1.4 mM M_E in 100 mM Tris-DCl buffer, pD = 8.0, with varying concentrations of $Fe(NO_3)_3$ unless otherwise stated (e.g., Figure S1 in Supporting Information). The pD adjustments were accomplished with NaOD and DCl. The standard correction of pD = pH + 0.4 was applied for all titrations in D_2O. The concentration of M_E was determined by spectrophotometric titration with a standardized stock solution of Fe(III): λ_{max} Fe(III)−M_E at 407 nm. The concentration of the Fe(III) stock solution, 0.0785 M $Fe(NO_3)_3$ in 0.036 M HNO_3 in D_2O, was determined spectrophotometrically with 1,10-phenanthroline: $Fe(phen)_3^{2+}$ λ_{max} 510 nm, ϵ = 11 000 M^{-1} cm^{-1}.[12] Fe(III) was added to M_E samples in four aliquots over 5 min, followed by vortexing and subsequent equilibration for at least one week prior to SANS measurements.

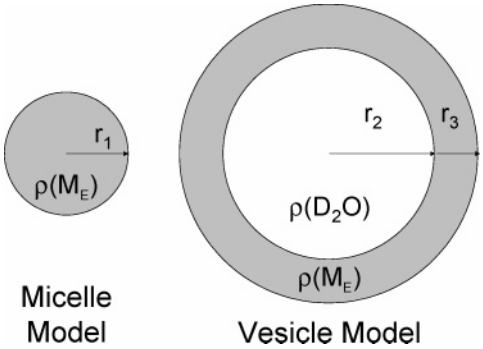

Figure 3. SANS models for micelles and vesicles. The micelle radius and vesicle core radius, r_1 and r_2, respectively, are allowed to be polydisperse according to a Shultz distribution.[14,15] Both models use the same SLD for M_E, labeled $\rho(M_E)$, and the SLD of the vesicle core, $\rho(D_2O)$, is fixed at the same value as that of the bulk solvent.

SANS Instrumentation. SANS experiments were conducted on the NSF-sponsored 30m NG3 SANS station at the NIST Center for Neutron Research (NCNR) in Gaithersburg, Maryland. An average neutron wavelength of 6 Å was used. Combining data from two different sample-to-detector distances (2 and 13 m) at a neutron wavelength of 6 Å allowed neutron wavevector transfers (Q) in the range of $0.004 < Q < 0.3$ $Å^{-1}$ to be accessed, in which $Q = (4\pi/\lambda)\sin(\theta/2)$, and θ represents the neutron scattering angle.

The two-dimensional (2-D) raw SANS intensity data were corrected for background radiation, and scatter from the cuvette containing the sample, and put on an absolute scale by a standard procedure that estimates the neutron flux at the sample.[13] The data were then circularly averaged to produce one-dimensional (1-D) SANS profiles of scattered neutron intensity, $I(Q)$, versus neutron wavevector transfer, Q.

SANS samples were loaded into quartz cuvettes (volume = 1.6 mL) with a path length of 5 mm and a window area of 3.2 cm^2. Each sample was run for at least 5 and 45 min at 2 and 13 m sample-to-detector distances, respectively, to obtain a minimum of 250 000 counts in each configuration. All SANS data were taken at room temperature.

Scattering Models. Least-squares fits to the SANS profiles were performed using Igor Pro (version 4.0.6.1) and software provided by the NCNR. Form factors for the model structures described below were convolved with the instrumental resolution (resulting from spread in λ, finite sample and detector pixel size, etc.) before being fit to the experimental data.

Two types of scattering models were used in this work (Figure 3), both of which are described in detail on the NCNR web site at http://www.ncnr.nist.gov/resources/. This site provides formulas for the relevant scattering form factors and polydispersity distributions as well as references to the original papers[14,15] in

(11) Harris, W. R.; Carrano, C. J.; Raymond, K. N. *J. Am. Chem. Soc.* **1979**, *101*, 2722−2727.

(12) Marczenko, Z. *Separation and Spectrophotometric Determination of Elements*; Ellis Horwood Limited: West Sussex, U.K., 1986; Chapter 27.

(13) Glinka, C. J.; Barker, J. G.; Hammounda, B.; Krueger, S.; Moyer, J. J.; Orts, W. J. *J. Appl. Crystallogr.* **1998**, *31*, 430−445.

(14) Griffith, W. L.; Triolo, R.; Compere, A. L. *Phys. Rev. A.* **1987**, *35*, 2200−2206.

Table 1. DLS Measurements of Vesicle Diameter and PI Values vs Fe(III)/M_E Ratio

Fe(III)/M_E ratio	1.1	1.2	1.5	2	2.7	3	3.4
diameter (nm)	193	180	176	190	212	190	206
PI value	0.27	0.24	0.23	0.25	0.27	0.26	0.27

which these formulas were first derived. The form factor for a solid sphere was used to fit SANS profiles obtained from micelles. The form factor of a hollow sphere was used to fit the scattering from vesicles. A linear combination of the sphere and hollow sphere models is used to describe SANS profiles obtained with solutions containing both micelles and vesicles. In both cases, polydispersity in the diameter of the molecular aggregates was described by a Shultz distribution function, as is common for SANS measurements of this type.[16] In all models, the level of incoherent neutron scattering was an adjustable parameter that was well determined by the data because sufficiently high values of wavevector transfer were measured. Absolute levels of incoherent background were as expected for samples in D_2O. For both solid and hollow sphere models, the difference in neutron scattering length density (SLD) between M_E and the solvent (D_2O) was calculated to be 4.12×10^{-6} Å^{-2} using the neutron SLD calculator available on the NCNR website. The solid and hollow sphere models are individually described below.

Micelle Model. Scattering from micelles was fitted with a form factor for a spherical particle with an average radius that was allowed to be polydisperse according to a Shultz distribution.[14] Samples are expected to contain a population of micelles of various diameters and shapes, and it is expected that both size and shape will fluctuate dynamically. The Shultz distribution incorporates such variations into the scattering function using a minimum number of parameters and a functional form that avoids unrealistic effects (such as negative particle radii). Nevertheless, the Shultz distribution is an approximation and should not be interpreted as evidence of a static distribution of micellar diameters. Since there are no correlations between particle positions at the low M_E concentrations used in this work, scattering from micelles is completely described by a form factor (i.e. the structure factor is set to unity for all scattering vectors).

Vesicle Model. Scattering from unilamellar vesicles is described by the form factor of a hollow spherical shell[15] with a neutron SLD that is equal to that of Fe(III)−M_E (2.21×10^{-6} Å^{-2}). The interior of the vesicle is taken to have an SLD of D_2O (6.33×10^{-6} Å^{-2}). The hollow-shell model allows for polydispersity of the radius of the hollow interior, but does not allow polydispersity of the shell thickness. Since the available Q range of the SANS measurements was not sufficient to accurately measure the diameter of the vesicles, we constrained the vesicle size and polydispersity to be the average of that obtained by the DLS measurements of samples containing Fe(III)/M_E ratios ranging from 1.1 to 1.5 (see results below; Table 1 and Supporting Information, Table S-1). This procedure yields improved confidence intervals for the other fitted parameters of our model.

Dynamic Light Scattering. DLS measurements were carried out on a Brookhaven BI-200SM goniometer with a AT9000 digital autocorrelator equipped with a Lexel 30 mW Ar laser ($\lambda = 633$ nm). The correlation function itself was calculated between delay times of 5 and 1×10^5 μs, and analyzed by the method of cumulants.[17] Measurements were taken in 12 mm round glass cells in a temperature-controlled toluene bath held at 25 °C with the detector set perpendicular (90°) to the incident laser beam. The diffusion coefficient was calculated using values of the viscosity and refractive index of D_2O at 25 °C (1.100 cP and 1.333, respectively). Measurements of particle size by DLS were repeated several times to obtain a standard deviation of ~4 nm for the hydrodynamic diameter. The DLS instrument used for these experiments cannot be used to characterize particles with diameters less than ~7 nm and thus could not be used to size the micelles encountered in this work; therefore DLS is only used to characterize the vesicles.

(15) Bartlett, P.; Ottewill, R. H. *J. Chem. Phys.* **1992**, *96*, 3306−3318.

(16) DeGiorgio, V.; Corti, M. *Physics of Amphiphiles − Micelles, Vesicles, and Microemulsions*; North-Holland: Amsterdam, 1983; p 69.

(17) Koppel, D. E. *J. Chem. Phys.* **1972**, *57*, 4814−4820.

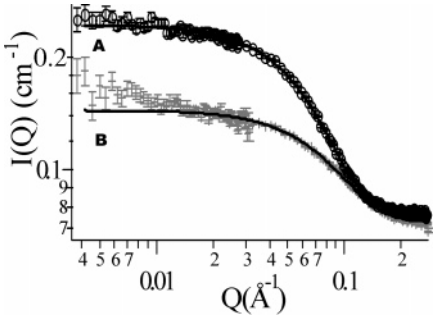

Figure 4. SANS profiles of apo and Fe(III)−M_E (1.4 mM) solutions demonstrating the decrease in micellar diameter upon Fe(III) chelation. (A) Apo-M_E, showing a best fit to micelles with a mean diameter of 4.0 (± 0.3) nm. (B) Fe(III)−M_E (i.e., Fe(III)/M_E = 1), showing a best fit to micelles with a mean diameter of 2.8 (± 0.3) nm.

Results

SANS of Apo-M_E. SANS data were collected for apo-M_E and fit to a scattering model for polydisperse solid spheres (Materials and Methods) (Figure 4A). At four different concentrations of apo-M_E (0.4−1.4 mM), a best fit to the SANS data was obtained by a population of spheres with an average diameter of 4.0 (± 0.3) nm and a polydispersity index (PI) of 0.3.[18] (The standard deviation was 0.1 nm when the PI was constrained and 0.3 nm when the PI was allowed to vary; see Supporting Information.) The size of these spheres relative to the molecular length of apo-M_E (~2.5 nm) is consistent with the formation of micelles. The fitted average diameter of the micelles varied little with apo-M_E concentration (i.e., less than 0.3 nm; Figure S-1 in Supporting Information), which is consistent with theoretical predictions that the molecular aggregation number of spherical micelles should vary only weakly with molecular concentration.[19] Since the average micelle diameter is relatively invariant with concentration, a single, concentration-independent average micelle diameter is entered in Table 2 for apo-M_E.

SANS of Fe(III)-M_E Complex. SANS data for the Fe(III)−M_E complex (i.e., Fe(III)/M_E ratio = 1) results in a significant reduction in SANS intensity as seen in Figure 4B. Since the CMCs for both apo-M_E and Fe(III)−M_E solutions are similar under the conditions studied in this work (~50 and ~75 μM, respectively),[7] the volume fractions of apo-M_E and Fe(III)−M_E aggregates are expected to be the same for solutions with the same surfactant concentration. For this reason, the decrease in SANS intensity for the Fe(III)−M_E solutions indicates a decrease in the size of the aggregates formed, not a decrease in volume fraction.

When Fe(III)−M_E SANS data were fit by the same solid sphere scattering model used to analyze SANS data for apo-M_E, a best fit was obtained with an average sphere diameter of 2.8 ± 0.3 nm and a PI of 0.35 (Supporting Information).[18] The smaller size of Fe(III)−M_E micelles relative to apo-M_E is also observed using size exclusion chromatography (data not shown).

(18) The Apo−M_E and Fe(III)−M_E samples in Figures 4−6 contain 3.4 mM trifluoroacetate (TFA) as a result of the isolation procedure, as determined by ^{19}F NMR referenced to hexafluorophosphate or 2,2,2-trifluoroacetamide. To investigate if TFA affects the results, SANS profiles for Apo−M_E and Fe(III)−M_E samples purified further to remove TFA were found to best fit a scattering model for 4.6 nm (PI = 0.23) and 3.7 nm (PI = 0.25) diameter micelles, respectively (i.e., slightly larger micelle diameters). However, the presence of TFA was not found to affect DLS results (which is a measure of the vesicle size) at all (i.e., particles with a hydrodynamic diameter of ~200 nm were formed in the presence or absence of TFA).

(19) Israelachvili, J. N.; Mitchell, D. J.; Ninham, B. W. J. *Chem. Soc., Faraday Trans. 2* **1976**, *72*, 1525−1568.

Table 2. Micelle and Vesicle Parameters for Various Fe(III)/M_E Ratios

fit parameters		apo-M_E	Fe(III)−M_E	Fe(III)/M_E ratio 1.1	1.2	1.5
micelle	diameter (nm)	4.0	2.8	2.8	2.8	2.8
	polydispersity	0.3	0.35	0.35	0.35	0.35
	% in micellar form			98	97	
vesicle	diameter (nm)	N/A	N/A	183	183	183
	polydispersity	N/A	N/A	0.25	0.25	0.25
	shell thickness (nm)	N/A	N/A	3.5	9.0	12.4
	% in vesicular form			2	3	
χ^2 value		1.2	1.0	1.2	1.6	3.8

The SANS profile of Fe(III)−M_E micelles (Figure 4B) shows a slight increase in scattered intensity at low Q ($Q < 0.015$ Å^{-1}), indicating the presence of a small population of large aggregates that are difficult to characterize due to their low concentration. Excluding the low Q data points that contain this slight increase in SANS intensity ($Q < 0.025$ Å^{-1}) from fits to the micelle scattering model does not significantly affect the fitted micelle parameters.

DLS of Fe(III)−M_E in the Presence of Excess Fe(III). DLS was used to investigate the large particles that form in the reaction of Fe(III)−M_E with excess Fe(III). DLS measurements on solutions of apo-M_E or Fe(III)−M_E do not indicate the presence of any large aggregates such as vesicles. However, when the Fe(III) concentration exceeds the apo-M_E concentration, a significant increase in turbidity is observed. Analysis of these solutions by DLS reveals the presence of particles with an average hydrodynamic diameter of 192 ± 13 nm and a PI range of 0.23−0.27 (i.e., average of 1.1 to 3.4 Fe(III)/M_E), depending on the amount of excess Fe(III) (Table 1 and Figure S-3, Supporting Information).[18]

Given the structural similarity between M_E and M_D and the observation of the vesicles in Fe(III)−M_D solutions by cryo-TEM at these concentrations (Figure 2),[7] the nature of the ∼200 nm diameter particles present in Fe(III)−M_E solutions is consistent with that of vesicles. Colloidal iron hydroxide was ruled out as the source of these large particles.[20] In addition, SANS data for Fe(III)−M_E containing an excess of iron is not well described by a scattering model based on a mixture of colloidal iron hydroxide and micelles (e.g., ∼200 nm polydisperse solid spheres plus 2.8 nm polydisperse solid spheres) judging from χ^2 values (i.e., 45, 138, and 704 for Fe(III)/M_E ratios of 1.1, 1.2, and 1.5, respectively). However, at Fe(III)/M_E ratios greater than 3, iron hydroxide precipitates,[21] and the turbidity of the supernatant decreases as a result of particle settling. In addition, the absorbance at 407 nm (i.e., λ_{max} of Fe(III)−M_E) also decreases because of the coprecipitation of Fe(III)−M_E.

SANS of Fe(III)-M_E in the Presence of Excess Fe(III). A striking change is observed in the SANS profiles of Fe(III)−M_E in the presence of excess Fe(III) (Figure 5) relative to the SANS profiles for apo-M_E and Fe(III)−M_E (Figure 4). The dramatically increased scattering at low values of Q indicates the presence of large molecular aggregates, which is consistent with DLS results as well as with our previous observation of vesicles by cryo-TEM for M_D (Figure 2).[7]

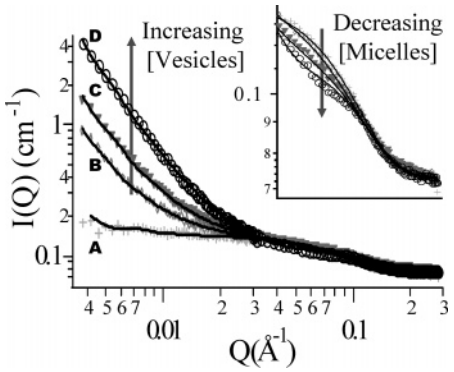

Figure 5. SANS profiles as a function of Fe(III)/M_E ratio demonstrating the presence of vesicles when the Fe(III)/M_E ratio exceeds 1.0. The concentration of apo-M_E was 1.4 mM. The ratios of Fe(III)/M_E are (A) 1.0, (B) 1.1, (C) 1.2, (D) 1.5. Inset: The reduction in intensity at Q values greater than ∼ 0.03 Å^{-1} indicates a reduction in micelle population with increasing iron concentration (the x-axis of the inset corresponds to values on the large plot directly below the inset).

The SANS data at excess iron concentration are fit by a model that includes both solid spherical particles (i.e., micelles) and much larger hollow spheres (i.e., vesicles). To fit the SANS data at excess Fe(III) (Figure 5B−D), the micelle diameter and PI value were constrained to that obtained from SANS measurements of Fe(III)−M_E micelles in the absence of excess Fe(III) (i.e., 2.8 ± 0.3 nm, PI = 0.35; Figure 4B), and the vesicle diameter and PI value were constrained to the average vesicle diameter obtained from DLS measurements of the 1.1, 1.2, and 1.5 Fe(III)/M_E samples, 183 ± 9 nm.[22] A best fit to the micelle-plus-vesicle model was obtained by minimizing χ^2 values with respect to the micelle and vesicle volume fraction as well as the vesicle shell thickness. The 10−20% excess molar Fe(III) over Fe(III)−M_E [i.e., in samples with Fe(III)/M_E ratios of 1.1 and 1.2] results in only a small percentage of the total volume fraction of Fe(III)−M_E assembling in vesicular form (i.e., 2 ± 0.5% at a ratio of 1.1 Fe(III)/M_E and 3 ± 0.1% at a ratio of 1.2). The results of the SANS fits are summarized in Table 2.

The fact that the value of χ^2 for an Fe(III)/M_E ratio of 1.1 is close to unity ($\chi^2 = 1.2$) is consistent with the assumption that the average size and polydispersity of the micelles does not change as vesicles begin to form. A best fit to the SANS data at 10% excess Fe(III) over Fe(III)/

(20) DLS analysis of Fe(III)−EDTA and Fe(III)−desferrioxamine B, neither of which are amphiphilic molecules, showed precipitation of iron hydroxide occurred at Fe(III)/ligand ratios greater than 1. The precipitate settled to the bottom of the cuvette within 48 h, which correlated with the anticipated loss of solution turbidity. In contrast, the turbidity of Fe(III)−M_E solutions with Fe(III)/M_E ratios greater than 1 was stable for over 6 months.

(21) Analysis of the orange precipitate by small-angle X-ray scattering, freeze fracture transmission electron microscopy, and conventional light microscopy gave no indication of a lamellar phase or other periodic structure. It is therefore believed that the orange precipitate is a mixture of amorphous Fe(III)−M_E and iron hydroxide.

(22) While DLS provides an independent and more accurate measure of the vesicle diameter, if the vesicle diameter and polydispersity are allowed to remain unconstrained while fitting SANS data at excess iron concentrations (e.g., Fe(III)/M_E ratios of 1.1, 1.2, and 1.5), the χ^2 values decrease by only ∼3% (see Supporting Information). Thus, both fitting methods are self-consistent. The fitted vesicle diameter and wall thickness change by less than 20% relative to fits in which the vesicle diameter and polydispersity are constrained and the fitted vesicle polydispersity ranges from 0.12 to 0.15.

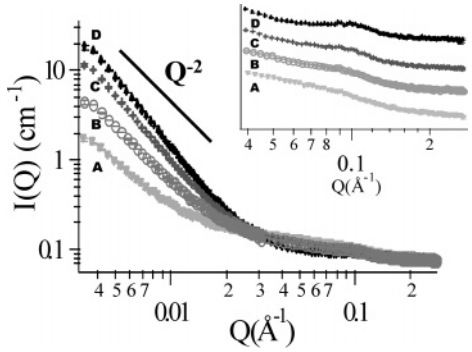

Figure 6. SANS profiles of Fe(III)−M_E in the presence of excess Fe(III) as a function of the Fe(III)/M_E ratio. The concentration of apo-M_E was 1.4 mM. The ratios of Fe(III)/M_E are (A) 1.2, (B) 1.5, (C) 2, (D) 3. The Q^{-2} dependence at low values of Q is shown. Inset: The development of a Bragg peak indicates a periodic structure with a repeat distance of ∼6 nm. SANS profiles are offset on the *y*-axis for clarity in this inset.

M_E (Figure 5B) is obtained with a vesicle shell thickness of 3.5 ± 0.7 nm, a reasonable value considering the maximum molecular length of Fe(III)−M_E is ∼2.5 nm and thus consistent with unilamellar vesicles.

As the relative excess of Fe(III) increases, the quality of the fit deteriorates based on χ^2 values, and the fitted vesicle shell thickness increases, perhaps indicating the formation of multilamellar aggregates. Above Fe(III)/M_E ratios of 1.2, the fitted volume fraction of the surfactant drops below levels expected for this concentration of Fe(III)−M_E,[23] and the micelle-plus-vesicle model is not used to analyze data for Fe(III)/M_E ratios of 2 and 3. An examination of SANS data for Fe(III)/M_E ratios of 2 and 3 reveals a Bragg-type peak at $Q = 0.1$ Å^{-1} (Figure 6 inset) that indicates a periodicity in the system of $2\pi/Q \approx 6$ nm. Such a periodicity is consistent with the hypothesis that vesicle walls are made up of multiple bilayers with a repeat distance of 6 nm. However, a possible transformation from a unilamellar vesicle phase to a stacked lamellae phase cannot be ruled out, and the deteriorating quality of the fits to a vesicle-plus-micelle model at large Fe(III) concentrations could reflect such a transformation. Future investigations will address whether stacked bilayer aggregates form at large excess Fe(III) concentration.

SANS data for samples with Fe(III)/M_E ratios of 2 and 3 (Figure 6) are also consistent with the presence of molecular aggregates with large, flat surfaces. Such aggregates could be vesicles or quasi-flat lamellae. The presence of such surfaces is confirmed by the approximate Q^{-2} dependence of the low-Q SANS intensity (Figure 6). If the scattering were from unilamellar or multilamellar vesicles, this power law would be expected for Q values greater than about 2π divided by the vesicle diameter and approximately up to 2π divided by the vesicle wall thickness.[24] Analysis of the low-Q SANS intensity of samples with Fe(III)/M_E ratios of 2 and 3 reveals that the SANS intensity decreases as $Q^{-2.08} \pm 0.03$ and $Q^{-2.13} \pm 0.03$, respectively. Although the low-Q SANS intensity for a vesicle with a perfectly rigid wall is expected to decrease as Q^{-2}, a slightly stronger Q dependence (i.e., steeper slope, Figure 6) could be attributable to undulations of a flexible vesicle wall.[25]

Scheme 1. Coordination of Fe(III) Could Give M_E a Larger Headgroup Area/Tail Volume Ratio Such that a Smaller Micelle Is Formed

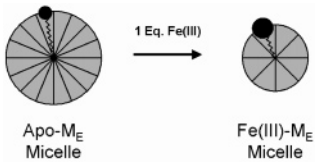

Scheme 2. The Headgroups of Fe(III)−M_E Bridged by Exogenous Fe(III) Could Pull the Headgroups Closer Together Resulting in a "Composite Surfactant" with a Lower Headgroup Area/Tail Volume Ratio that May Drive Vesicle Formation

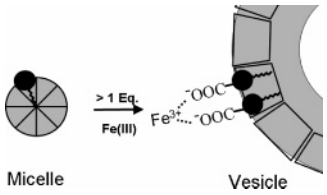

Discussion

The SANS and DLS results suggest that this microbially produced amphiphilic siderophore, M_E, and very possibly other amphiphilic siderophores, assemble in solution to form micelles that decrease in diameter upon coordination of the first equivalent of Fe(III) to the peptide headgroup, (i.e., 4.0 and 2.8 nm for apo-M_E and Fe(III)−M_E micelles, respectively; Figure 4), and that the interaction of Fe(III)−M_E micelles with excess Fe(III) induces an MVT. Since the charge of apo-M_E does not change upon coordination of Fe(III) at pD 8.0,[26] the decrease in micellar diameter upon Fe(III) addition is likely due to a change in molecular geometry upon iron coordination. The ratio of the headgroup area-to-tail volume for M_E could increase upon Fe(III) coordination, giving it a more conical geometry that can cause a decrease in the diameter of the micelle (Scheme 1).[19] Considering the geometry of a spherical micelle, this relationship can be expressed as

$$R = 3\,v/a$$

in which R is the radius of the micelle, v is the hydrocarbon tail volume, and a is the area of the surfactant headgroup. This analysis is consistent with previous results on the greater partitioning of apo-M_E into synthetic dimyristoylphosphatidylcholine vesicles compared to partitioning by Fe(III)−M_E.[27]

The addition of excess Fe(III) to Fe(III)−M_E induces a phase change in which a portion of the Fe(III)−M_E micelles rearrange into unilamellar vesicles (i.e., at the small excess of Fe(III)/M_E = 1.1; Figure 5B, Table 2), as well as multilamellar aggregates (i.e., at Fe(III)/M_E ≥ 1.2; Figure 5C,D, Figure 6). Previous studies with synthetic metal-

(23) The fitted volume fraction of surfactant in the Apo−M_E, Fe(III)−M_E, Fe(III)/M_E = 1.1, and Fe(III)/M_E = 1.2 samples (Figures 4A,B and 5B,C, respectively) are all the same (i.e., within 5%) and in reasonable agreement with the calculated volume fraction (see Supporting Information). However for Fe(III)/M_E ratios of 1.5, 2, and 3, the fitted volume fraction of surfactant is 85%, 81%, and 55% of the value obtained for the Fe(III)−M_E sample, respectively. This decrease in fitted volume fraction is not reasonable considering the fact that the absorbance at 407 nm (i.e., the λ_{max} of Fe(III)−M_E) for all of these solutions is the same as that for the Fe(III)−M_E sample, indicating that the Fe(III)−M_E concentration is also the same.

(24) Porod, G. In *Small Angle X-ray Scattering*; Glatter, O., Kratky, O., Eds.; Academic Press: London, 1982; p 17.

(25) Ho, D. L.; Briber, R. M.; Glinka, C. *J. Chem. Mater.* **2001**, *13*, 1923−1931.

(26) Apo−M_E loses three protons upon Fe(III) coordination; thus at the near neutral pH of these experiments, Apo−M_E and Fe(III)−M_E each have an overall charge of −1, as a result of the deprotonated terminal carboxylate.

(27) Xu, G.; Martinez, J. S.; Groves, J. T.; Butler, A. *J. Am. Chem. Soc.* **2002**, *124*, 13408−13415.

Scheme 3. Phase Behavior of M_E as a Function of Fe(III)/M_E Ratio

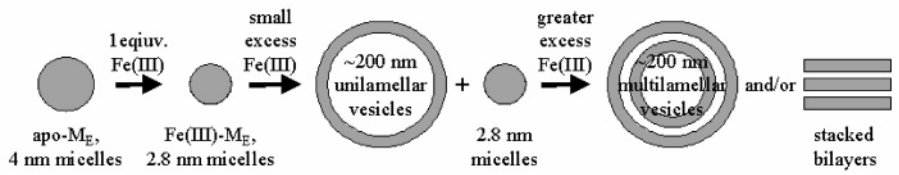

chelating amphiphiles reveal that an MVT can result from the coordination of a transition metal ion to multiple surfactant headgroups.[1−3] Bridging the headgroups of multiple surfactants by the metal ion effectively produces a composite surfactant molecule with two or more alkyl tails.[1−5] Surfactants with multiple alkyl tails have a more rodlike geometry that favors a vesicular arrangement, whereas cone-shaped monocephalic surfactant molecules are thermodynamically predisposed to form micelles.[19] A similar mechanism could stabilize Fe(III)−M_E vesicles in which the excess Fe(III) could bind to the terminal carboxylate moiety of multiple Fe(III)−M_E headgroups producing an iron-bridged complex with two or three alkyl tails that will preferentially aggregate as a vesicle instead of a micelle (Scheme 2). Furthermore, bridging multiple carboxylates with Fe(III) could also serve to screen the electrostatic repulsion between neighboring Fe(III)−M_E headgroups. Reducing the anionic repulsion between Fe(III)−M_E headgroups would enable closer packing and could provide an additional impetus for vesicle formation.

In addition to allowing multiple Fe(III)−M_E headgroups to pack closer together, coordination of excess Fe(III) by the anionic terminal carboxylate of the Fe(III)−M_E peptide decreases the overall negative charge of the bilayer. The decrease in charge of unilamellar vesicle bilayers could, in turn, induce the formation of multilamellar vesicles or stacks of lamellae by decreasing the repulsive force between anionic bilayers.[28] Coordination of excess Fe(III) to terminal carboxylates on the aggregate surface could also be accompanied by indirect solvent-ordering effects (e.g., in terms of the lyotropic Hofmeister series)[29−30] that play a role in the phase behavior of Fe(III)−M_E; however, the relative importance of metal coordination versus electrostatic effects is not known yet. An overall schematic of the phase behavior of M_E as a function of Fe(III) concentration is illustrated in Scheme 3.

Suites of amphiphilic siderophores are produced by a wide variety of marine bacteria,[7,8] and appear to be more widespread than those found to be produced by terrestrial bacteria.[8] The self-assembly processes exhibited by other amphiphilic siderophores has not yet been investigated, although some amphiphilic siderophores have analogous chemical structures with anionic headgroups and may exhibit aggregation behavior similar to that of M_E. Understanding the mechanism by which M_E undergoes an MVT is thus important, not only from a molecular point of view to elucidate the factors that drive the MVT, but also from a physiological point of view. One can imagine many advantageous scenarios by which bacteria could use the iron-dependent phase behavior of amphiphilic siderophores in the iron acquisition process. In fact, other cationic metal ions are present in the ocean at greater concentrations than iron and may also induce the MVT after the first equivalent of Fe(III) coordinates to M_E. Thus, the effect of other metal ions on the MVT, as well as the self-assembly processes displayed by the other amphiphilic siderophores, including the whole suite of marinobactins, is under investigation.

Acknowledgment. We acknowledge the support of the National Institute of Standards and Technology, U.S. Department of Commerce, in providing the neutron research facilities used in this work. This work utilized facilities supported in part by the National Science Foundation under Agreement No. DMR-9986442. We particularly thank Dr. Boualem Hammouda for helpful discussions. We also gratefully acknowledge support from NIH GM38130 (A. B.), NSF NIRT grant CHE0103516 (A. B.), NSF EMSI grant CHE0221978 (A. B.), and US Department of Energy contract W-7405-ENG-36 with the University of California (R. P.).

Supporting Information Available: Dependence of micelle volume fraction and diameter on micelle polydispersity; dependence of micelle-plus-vesicle model parameters on vesicle diameter and polydispersity; and dependence of solution turbidity on iron concentration. This material is available free of charge via the Internet at http://pubs.acs.org.

LA0519352

(28) Molina, F.; Llácer, C.; Vila, A. O.; Puchol, A.; Figueruelo, J. *Colloids Surf. A*, **1998**, *140*, 91−101.
(29) Cacace, M. G.; Landau, E. M.; Ramsden, J. J. *Q. Rev. Biophys.* **1997**, *30*, 241−277.
(30) Collins, K. D. *Methods* **2004**, *34*, 300−311.